Assessing the complementary role of Surface Flux Equilibrium (SFE) theory and Maximum Entropy Production (MEP) principle in the estimation of actual evapotranspiration

Yeonuk Kim[1*], Monica Garcia[2], T. Andrew Black[3], and Mark S. Johnson[1, 4]

[1]Institute for Resources, Environment and Sustainability, University of British Columbia; Vancouver, V6T1Z4, Canada.

[2] Research Centre for the Management of Agricultural and Environmental Risks (CEIGRAM). E.T.S.I. Agronomica, Alimentaria y de Biosistemas. Universidad Politecnica de Madrid, Spain.

[3] Faculty of Land and Food Systems, University of British Columbia; Vancouver, V6T1Z4, Canada.

[4] Department of Earth, Ocean and Atmospheric Sciences, University of British Columbia; Vancouver, V6T1Z4, Canada.

Corresponding author: Yeonuk Kim (yeonuk.kim.may@gmail.com)

Key Points:

- We propose a model to estimate evapotranspiration, which can represent both land-atmosphere equilibrium and non-equilibrium.
- The proposed model improves the performance of evapotranspiration estimation compared to the surface flux equilibrium approach.
- The proposed model does not require any empirical parameters and only uses readily obtainable meteorological variables.

Abstract

Although evapotranspiration (ET) from the land surface is a key variable in Earth systems models, the accurate estimation of ET based on physical principles remains challenging. Parameters used in current ET models are largely empirically based, which could be problematic under rapidly changing climatic conditions. Here, we propose a physically-based ET model that estimates ET based on the surface flux equilibrium (SFE) theory and the maximum entropy production (MEP) principle. We derived an expression for aerodynamic resistance based on the MEP principle, then propose a novel ET model that complementarily depends on the SFE theory and the MEP principle. The proposed model, which is referred to as the SFE-MEP model, becomes equivalent to the MEP state in non-equilibrium conditions when turbulent mixing is weak and the land surface is dry. On the contrary, the SFE-MEP model is similar to ET estimation based on the SFE theory in other conditions meeting land-atmosphere equilibrium. This feature of the SFE-MEP ET model allows accurate ET estimation for most inland regions by incorporating both equilibrium and non-equilibrium characteristics of the atmospheric boundary layer. As a result, the SFE-MEP model significantly improves the performance of SFE ET estimation, particularly for arid regions. The proposed model and its high accuracy in ET estimation enable novel insight into various Earth system models as it does not require any empirical parameters and only uses readily obtainable meteorological variables including reference height air temperature, relative humidity, available energy, and radiometric surface temperature.

Plain Language Summary

Terrestrial evaporation, also known as evapotranspiration (ET), is a central variable controlling the water, energy, and carbon cycles. However, it is difficult to estimate ET from physical principles due to complex interactions between the land and the atmosphere. An emerging theory of surface flux equilibrium suggests that atmospheric observations reflect land surface conditions owing to a land-atmosphere coupling, making it possible to estimate ET only using meteorological information. Nevertheless, we demonstrate that if the equilibrium is not achieved within several days, particularly in dry regions, the emerging surface flux equilibrium theory cannot properly estimate ET. We resolve this problem by introducing the maximum entropy production principle, a thermodynamic principle that can be applicable to non-equilibrium conditions. By combining two theories with complementary relationships, we significantly improve ET estimation performance. In our approach, empirical and adjustable parameters are not required and ET can be easily estimated based on a land-atmosphere coupling by using meteorological information and land surface temperature.

1 Introduction

Actual evaporation, also referred to as evapotranspiration (ET, sum of soil evaporation, intercepted water evaporation and plant transpiration) over the land surface plays an important role in the water cycle, the land surface energy balance, and even the carbon cycle (K. Wang & Dickinson, 2012). Accordingly, modelling ET is one of the key components of hydrologic and Earth systems modelling (J. M. Chen & Liu, 2020; Cuxart & Boone, 2020; Fisher et al., 2017; Katul et al., 2012; K. Wang & Dickinson, 2012). However, ET is difficult to estimate or spatiotemporally upscale from measurements due to its complex interactions with the atmosphere and heterogeneous surface conditions. Therefore, estimating ET from available information is a key challenge and of great interest in many water-related disciplines.

Several approaches to estimate ET have been proposed including land surface models (e.g., Lawrence et al., 2020), empirical machine learning models (e.g., Jung et al., 2019), and satellite remote sensing-based models (e.g., J. M. Chen & Liu, 2020). Although detailed processes constraining ET in each model vary significantly, most ET models try to represent physical processes driving evaporation to be robust across any region and time period (i.e., past and future). Representation of physical processes is particularly important under rapidly changing climatic conditions in order to correctly determine future ET trends and projections. Thus, fully physically-based ET measurements and estimations are commonly used as benchmarks for evaluating data-driven and other models (Pan et al., 2020). Furthermore, several empirical machine learning ET models try to incorporate physical processes to yield more realistic results (Koppa et al., 2022; Reichstein et al., 2019).

ET models based on mass-transfer theory (or Monin-Obukhov similarly theory: MOST) such as land surface models, Penman-Monteith based models, and thermal remote sensing-based surface energy balance models are commonly considered to be physically-based models. Rigorously speaking, however, parameters used in the mass-transfer theory are not completely based on first principles and rely on the semi-empirical parameterization of aerodynamic resistance (or aerodynamic conductance) due to the complex nature of turbulence (Kleidon & Renner, 2018; Lee, 2018). Uncertainty in the parameterization of aerodynamic resistance causes bias in ET estimation, particularly in surface energy balance models which rely largely on aerodynamic resistance (Mallick et al., 2018; Trebs et al., 2021). Furthermore, in Penman-Monteith as well as in land surface models, semi-empirical parameterization representing surface conditions at a given time such as surface resistance is a primary source of uncertainty (Polhamus et al., 2013; Short Gianotti et al., 2019). Therefore, it is difficult to determine ET solely based on the first principles in these conventional approaches, despite commonly considered as physically-based approaches (Kleidon & Renner, 2018).

Alternatively, a few related concepts from thermodynamics have been proposed to physically constrain turbulent heat fluxes (e.g., Conte et al., 2019; J. Wang & Bras, 2011). Among them, the recently introduced surface flux equilibrium (SFE) theory representing land-atmosphere coupling is of great interest in that it can simply estimate ET using only meteorological information and available energy (McColl et al., 2019). This simple model quite successfully estimates actual ET at daily and multi-day time scales without any surface constraints or empirical parameters (S. Chen et al., 2021; McColl & Rigden, 2020). Yet, the SFE approach overestimates ET when ET is very low and underestimates it when ET is very high, implying that potential room for improvement exists (McColl & Rigden, 2020). By introducing the PM_{RH} equation (Penman-Monteith equation expressed using relative humidity), Kim et al.

(2021) explicitly showed that SFE-based ET estimates can diverge from actual ET when vertical gradients of relative humidity from the land surface to the atmosphere are large. This finding provided the motivation for this present study.

Here, we extend SFE theory in order to accurately estimate ET for various environmental conditions without any empirical parameterization by employing the maximum entropy production (MEP) principle, a thermodynamic principle for non-equilibrium conditions (Kleidon & Schymanski, 2008). In the proposed model, we merge SFE theory and the MEP principle with complementary characteristics, which improves the accuracy of the resulting ET estimation. Also, our proposed model only requires reference height air temperature and relative humidity, available energy, and radiometric surface temperature (which can be calculated from outgoing longwave radiation or obtained from thermal remote sensing).

This study is structured as follows. First, we theoretically identify the conditions when SFE theory does not work well. To do this, we employ a simple closed box model of the atmospheric boundary layer (ABL). Then, we introduce the MEP principle that can be used when the SFE theory does not work well. Next, we propose a simple yet physically-based ET estimation which stems from the complementary role of the SFE theory and the MEP principle. We refer to the proposed model as the SFE-MEP model. Finally, we validate our approach using in-situ ET observations from eddy-covariance tower sites contained in the FLUXNET2015 dataset (Pastorello et al., 2020).

2 Theory

2.1 When does SFE theory not work well?

McColl et al. (2019) showed that the SFE state is achieved when moistening and heating at the land surface become equivalent in the RH budget. In this state, latent heat flux (LE in units of W m^{-2}) can be simply determined as follows.

$$LE = \frac{RH_a s}{RH_a s + \gamma}(R_n - G) \quad (1)$$

where $s(=\frac{\partial q^*}{\partial T})$ is the linearized slope of saturation specific humidity versus temperature (kg water vapour (kg moist air)$^{-1}$ K^{-1}), γ is psychrometric constant (K^{-1}), R_n is net radiation (W m^{-2}), G is soil heat flux (W m^{-2}), RH_a is relative humidity at a reference height, and R_n - G is available energy at the land surface. LE is the product of the latent heat of vaporization (L) and the evapotranspiration (ET) rate on a mass per unit land area basis (E).

Using sensitivity tests, McColl et al. (2019) provided evidence that most initial conditions defined for an idealized ABL box evolve toward the SFE state within several days. Nevertheless, they did not provide a explicit solution for LE, unlike previous studies addressing traditional equilibrium evaporation (McNaughton & Spriggs, 1986; Raupach, 2001). Therefore, it is difficult to intuitively understand how LE evolves toward the SFE state.

To explicitly derive the solution yielding the SFE state, we revisit an idealized and closed ABL box model, which further simplifies the approach used by McColl et al. (2019). Following McColl et al. (2019), we consider an idealized ABL box model that can be interpreted as the daily averaged ABL with constant available energy input and constant aerodynamic resistance

(Figure A1 in Appendix A). Unlike McColl et al. (2019), we ignore the relaxation heat fluxes at the top of the ABL to simplify the ABL system following traditional equilibrium models (McNaughton & Jarvis, 1983; Raupach, 2001). This simplification is justified in that relaxation conductance at the top of the ABL is much smaller than aerodynamic conductance at the land surface at the multi-day time scale (McColl et al., 2019). The sensible and latent heat budgets for the closed ABL box model can be written as follows.

$$\frac{d\theta_m}{dt} = \frac{H}{\rho c_p h} \tag{2}$$

$$\frac{dq_m}{dt} = \frac{\gamma LE}{\rho c_p h} \tag{3}$$

where h is the ABL box height (m), t is time, ρ is the air density (kg m^{-3}), c_p is the specific heat capacity of air at constant pressure (J kg^{-1} K^{-1}), θ_m is the mean potential temperature in the ABL (K), and q_m is the mean specific humidity in the ABL (kg water vapour (kg moist air)$^{-1}$). H and LE are sensible and latent heat fluxes at the land surface (W m^{-2}).

In Appendix A, we provide a derivation of an expression for LE using Equations 2 and 3. In this derivation, we parameterize land surface dryness using the land surface relative humidity instead of the "big-leaf" surface resistance following Kim et al. (2021). This difference in the surface parameterization provides a different steady state evaporation from the traditional equilibrium evaporation (McNaughton & Jarvis, 1983). The resulting solution is as follows:

$$LE = \frac{RH_a s}{RH_a s+\gamma}(R_n - G) + [LE|_{t=0} - \frac{RH_a s}{RH_a s+\gamma}(R_n - G)]exp(\frac{-t}{\tau}) \tag{4}$$

where $LE|_{t=0}$ is the initial evaporation, and τ is the time constant of the approach to steady state given as follows

$$\tau = \frac{q^*(T_0)(RH_0 s+\gamma)}{q^*(\theta_m)(RH_a s+\gamma)} hr_a \tag{5}$$

where r_a is the aerodynamic resistance to heat and water vapour transfer (s m^{-1}), T_0 is the land surface temperature, and RH_0 is the land surface relative humidity.

Equation 4 demonstrates how LE evolves toward the SFE state. Since τ is a positive integer, the second term of the right-hand side of Equation 4 approaches zero with time, and thus LE asymptotically approaches $\frac{RH_a s}{RH_a s+\gamma}(R_n - G)$. This resulting steady state is exactly the same as the SFE state.

The time scales required for the closed ABL box to approach its steady state vary with τ in Equation 5. If τ is large, the length of time required to reach quasi steady state is large (McNaughton & Jarvis, 1983; McNaughton & Spriggs, 1986; Raupach, 2000). For most inland regions, $\frac{q^*(T_0)(RH_0 s+\gamma)}{q^*(\theta_m)(RH_a s+\gamma)}$ in Equation 5 is close to 1.1 as we found in our recent study (Kim et al., 2021). In these typical conditions, τ becomes $1.1hr_a$ in Equation 5. This suggests that the time scale required for the SFE state is determined by the ABL depth and by turbulent mixing. As shown by McColl et al. (2019), various combinations of h and r_a allow the steady state within several days.

Nevertheless, we can imagine large τ in some extreme conditions, which make it difficult to approach steady state within several days. When the land surface is very dry (e.g., desert), the

ABL depth can be up to 4 km, much higher than typical conditions. Also, over very dry regions, vegetation cover is minimal and thus the aerodynamic roughness of the land surface is low, which results in weak turbulent mixing (i.e., large r_a). When turbulent mixing is weak, the temperature difference between the land surface and the atmosphere can increase substantially leading to a large $\frac{q^*(T_0)}{q^*(\theta_m)}$. Therefore, every component of τ in Equation 5 (i.e., $\frac{q^*(T_0)(RH_0 s+\gamma)}{q^*(\theta_m)(RH_a s+\gamma)}$, h, and r_a) reaches its maximum when the land surface is extremely dry. In this large τ condition over arid regions, the length of time required to reach quasi steady state increases substantially. Therefore, the ABL system cannot approach steady state within several days if the land surface is very dry and turbulent mixing is weak. In other words, the SFE theory estimating ET cannot properly determine ET for arid regions due to this non-equilibrium. Indeed, a recent study found the lowest performance of the SFE theory for very dry regions (S. Chen et al., 2021), supporting this theoretical evaluation. This is also further confirmed by our results in the result section. Therefore, in order to overcome the limitations of the SFE theory, we need an alternative theory for dry regions where SFE theory does not perform well in terms of ET estimation.

2.2 A solution to non-equilibrium: the MEP principle

The theoretical evaluation in the previous section is consistent with empirical findings that demonstrate the the SFE theory cannot accurately estimate ET in dry regions (S. Chen et al., 2021). We demonstrate that the ABL over very dry regions cannot approach the equilibrium state, even within a period of several days. Therefore, we need an alternative physical principle to better estimate turbulent heat fluxes under non-equilibrium conditions. The principle of maximum entropy production (MEP) could be an alternative approach for non-equilibrium conditions. This is because the MEP principle suggests that a system far from equilibrium tends to organize in a way that the entropy production rate is maximized at steady state (Kleidon & Schymanski, 2008).

Here, we employ the MEP principle to estimate the aerodynamic resistance (or conductance as the reciprocal of resistance) for dry conditions when sensible heat flux is dominant and SFE theory does not work well. We estimate aerodynamic resistance based on the entropy production equation introduced by Kleidon and Schymanski (2008), which is independent of the MOST theory. It should be noted that our work is different from some MEP-related previous studies (J. Wang & Bras, 2010; J. Wang & Bras, 2011), which were based on the MEP formalism presented by Dewar (2005).

We start by writing the energy balance equation at a single leaf for a condition for which there is no evaporation.

$$g_a \rho c_p (T_0 - T_a) = R_{sn} + \varepsilon Rl_{atm} + \varepsilon Rl_{soil} - 2\varepsilon\sigma_{SB} {T_0}^4 \quad (6)$$

where g_a is aerodynamic conductance (m s^{-1}), T_0 is leaf surface temperature (K), T_a is near-leaf air temperature (K), R_{sn} is shortwave net radiation at the single leaf (W m^{-2}), Rl_{atm} is downward longwave radiation from the atmosphere to the leaf (W m^{-2}), Rl_{soil} is upward longwave radiation from the soil below the leaf (W m^{-2}), ε is leaf surface emissivity, and σ_{SB} is Stefan-Boltzmann constant (W m^{-2} K^{-4}). In Equation 6, the left-hand side represents turbulent sensible heat flux from the leaf surface to the air while the right-hand side represents the radiation budget (i.e., net radiation). The last term of the right-hand side represents the sum of outgoing longwave

224 radiation from the leaf to the atmosphere (upward) and to the soil (downward). We express net
225 radiation at a single leaf instead of the land surface to faithfully represent the role of T_0 in
226 emitting heat energy while ignoring soil heat flux which is difficult to calculate without knowing
227 soil thermal conductivity and heat capacity.

228 In order to effectively solve Equation 6 for the MEP state, we only consider g_a and T_0 as
229 variables while others are constants although they interact with T_0 through radiative feedback.
230 Following isothermal net radiation introduced by Monteith (1981), we rewrite Equation 6 as
231 follows to substitute T_0 by T_a:

232 $$g_a \rho c_p (T_0 - T_a) = R_{sn} + \varepsilon R l_{atm} + \varepsilon R l_{soil} - 2\varepsilon\sigma_{SB} {T_a}^4 - 2\varepsilon\sigma_{SB}({T_0}^4 - {T_a}^4)$$

233 $$g_a \rho c_p (T_0 - T_a) + 8\varepsilon\sigma_{SB} {T_a}^3 (T_0 - T_a) = R_{sn} + \varepsilon R l_{atm} + \varepsilon R l_{soil} - 2\varepsilon\sigma_{SB} {T_a}^4 \quad (7)$$

234 Here, the second term of the left-hand side of the resulting Equation 7 is the longwave radiative
235 correction using a linear approximation (i.e., ${T_0}^4 - {T_a}^4 \approx 4{T_a}^3 (T_0 - T_a)$), which is introduced
236 since ${T_a}^4$ replaces ${T_0}^4$ (Monteith, 1981).

237 Equation 7 can be rearranged to obtain an expression for $T_0 - T_a$ as follows

238 $$T_0 - T_a = \frac{R_{ni}}{g_a \rho c_p + 8\varepsilon\sigma_{SB} {T_a}^3} \quad (8)$$

239 where $R_{ni} (= R_{sn} + \varepsilon R l_{atm} + \varepsilon R l_{soil} - 2\varepsilon\sigma_{SB} {T_a}^4)$ is isothermal net radiation.

240 According to Kleidon and Schymanski (2008), entropy production (σ) (W m^{-2}K^{-1}) by
241 sensible heat flux (H) can be expressed as follows:

242 $$\sigma = H\left(\frac{1}{T_a} - \frac{1}{T_0}\right) \approx H \frac{T_0 - T_a}{{T_a}^2} \quad (9)$$

243 where temperature is in K. Equation 9 can be rewritten by using Equation 8 and the aerodynamic
244 expression of sensible heat flux (i.e., $H = g_a \rho c_p (T_0 - T_a)$) as follows:

245 $$\sigma = \frac{g_a \rho c_p}{{T_a}^2} \left(\frac{R_{ni}}{g_a \rho c_p + 8\varepsilon\sigma_{SB} {T_a}^3}\right)^2 \quad (10)$$

246 Equation 10 provides a relationship between the entropy production and g_a for given
247 values of R_{ni} and T_a. We illustrate this relationship in Figure 1. This illustration demonstrates
248 that while the temperature difference (i.e., $T_0 - T_a$) increases with decreasing g_a reaching a finite
249 maximum value at $g_a = 0$, there is a maximum σ state (i.e., MEP) with respect to $g_a (>0)$ for a
250 given meteorological condition. In Figure 1, σ reaches its maximum when g_a is approximately
251 0.0011 m s^{-1} (or aerodynamic resistance, r_a is approximately 90 s m^{-1}). This condition can be
252 defined as the MEP state.

253 Mathematically, this MEP state state can be determined by calculating the partial
254 derivative of Equation 10 with respect to g_a. That is, $\frac{\partial\sigma}{\partial g_a} = 0$ is equivalent to the MEP state, and
255 the solution for $\frac{\partial\sigma}{\partial g_a} = 0$ is (detailed derivation in Appendix B):

256 $$g_{MEP} = \frac{1}{r_{MEP}} = \frac{8\varepsilon\sigma_{SB} {T_a}^3}{\rho c_p} \quad (11)$$

where g_{MEP} and r_{MEP} are the aerodynamic conductance (m s^{-1}) and aerodynamic resistance (s m^{-1}), respectively, that yield the MEP state. Equation 11 shows that aerodynamic conductance (or resistance) for the MEP state is determined using only absolute temperature.

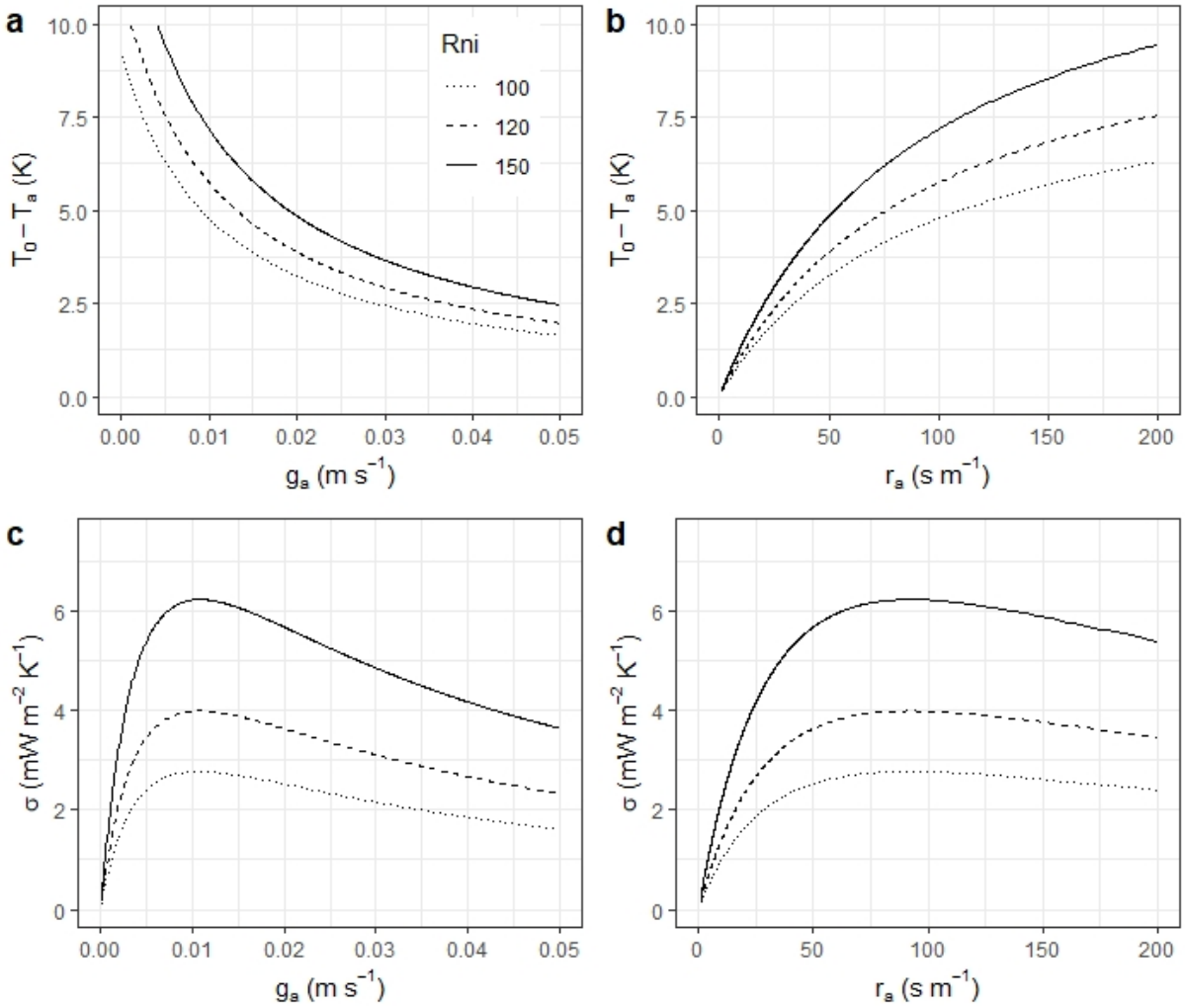

Figure 1. Temperature difference (a and b) and entropy production (c and d) as a function of aerodynamic conductance (a and c) and aerodynamic resistance (b and d). Here, Equations 8 and 10 are used to show this relationship with ρ = 1.2 kg m^{-3}, c_p = 1.01 J $g^{-1}K^{-1}$, T_a = 288.15 K, and varying R_{ni} (100, 120, and 150 W m^{-2}).

Is this theoretical derivation for g_{MEP} and r_{MEP} also empirically meaningful although it is independent to wind speed? To confirm the robustness of Equation 11, we compute g_{MEP} and r_{MEP}, and validate them in Figure 2 using daily turbulent heat fluxes observations contained in the FLUXNET2015 database (Pastorello et al., 2020) (details for the dataset are provided in the Methods section). We used values of observed sensible heat flux, air temperature, and radiometric surface temperature to calculate aerodynamic conductance and resistance as $g_a =$

$\frac{H}{\rho c_p(T_0-T_a)}$ and $r_a = \frac{\rho c_p(T_0-T_a)}{H}$ (details of the calculation of the radiometric surface temperature (T_0) are provided in the next section). We compare calculated aerodynamic conductance (or resistances) and g_{MEP} (or r_{MEP}) values in Figure 2 by selecting conditions for which H is dominant ($LE < 10$ W m^{-2} and $H > 50$ W m^{-2}).

As shown by Figure 2, when the entropy production (σ) is low compared to theoretical maximum (σ_{MEP}: derived by substitituing Equation 11 into Equation 10), g_{MEP} underestimates the measured g_a values and r_{MEP} overestimates observed aerodynamic resistance. However, when σ approaches its maximum, observed g_a (or r_a) approaches g_{MEP} (or r_{MEP}). This result demonstrates the robustness of Equation 11 in determining aerodynamic conductance or resistance for the MEP state without requiring any conceptual or empirical parameters and wind speed information.

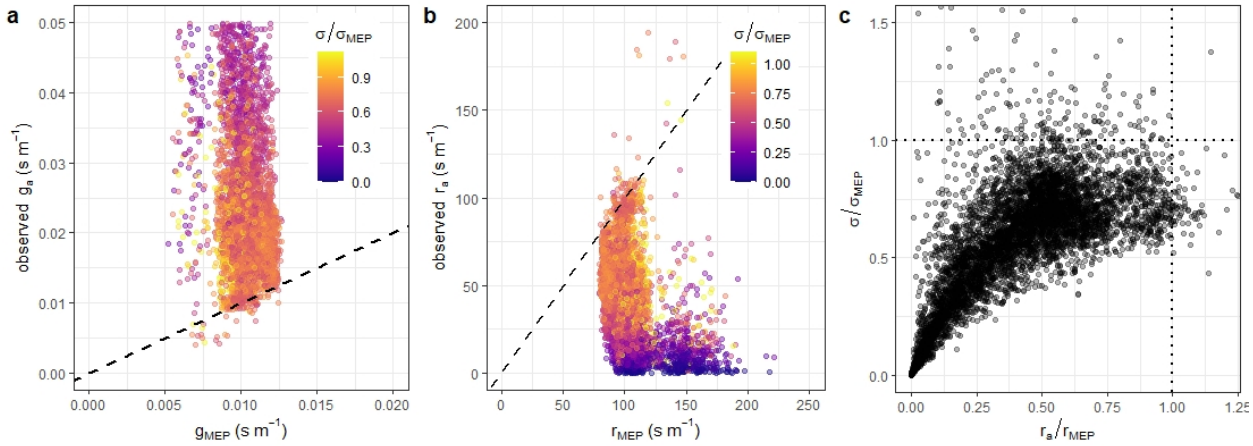

Figure 2. Validation of Equation 11. (a) relationship between between g_{MEP} and observed g_a. (b) relationship between r_{MEP} and observed r_a. (c) relationship between normalized r_a and σ by their respective MEP states. Here, we only include daily scale data points when sensible heat flux is dominant ($LE < 10\ W\ m^{-2}$ and $H > 50\ W\ m^{-2}$). In panels (a) and (b), color represents entropy production relative to its maximum and the dashed lines are one-to-one lines for the respective panels. In panel (c), the dotted lines indicate conditions for which the normalized ratios are unity.

2.3 Proposed model: the SFE-MEP model

In the previous sections, we presented two independent theories that can constrain surface heat fluxes: SFE and MEP. The SFE theory works for the well-mixed equilibrium ABL particularly over wet or moderate-wet land surfaces, while the MEP theory can be applied to the non-equilibrium ABL over dry land surfaces. Is it the case that real world ABL and the surface heat fluxes are simultaneously affected by the mechanisms underpinning these two physical theories? In this section, we propose an additive model that merges the SFE theory and the MEP principle with complementary characteristics.

We propose a novel partitioning of sensible heat flux as follows:

$$H = H_{SFE} + H_{MEP} \quad (12)$$

where

$$H_{SFE} \equiv \frac{\gamma}{RH_a s} LE \quad (13)$$

$$H_{MEP} \equiv \rho c_p \frac{T_0 - T_a}{r_{MEP}} \quad (14)$$

Substituting the Equation 12 into the energy balance equation (i.e., $H + LE = R_n - G$) and arranging it for LE yields.

$$LE = \frac{RH_a s}{RH_a s + \gamma}(R_n - G - H_{MEP}) \quad (15)$$

Equation 15 is the proposed ET estimation model. This combinatory sensible heat flux model can blend SFE theory with the MEP principle. For a well-mixed system where $T_0 - T_a$ is small and r_{MEP} is much larger than true aerodynamic resistance due to strong turbulent mixing, H_{MEP} becomes negligible (Equation 14), with H converging to H_{SFE}. This condition is exactly equivalent to the SFE theory since Equation 15 becomes equivalent to Equation 1. On the other hand, when turbulent mixing is weak and the system is dry, H_{MEP} becomes much larger than H_{SFE}, and thus H is close to H_{MEP}. This condition is equivalent to the MEP state. Therefore, the proposed can reconcile and explain two physical theories without any conflict.

According to the PM_{RH} (Penman-Monteith using RH) equation introduced by Kim et al. (2021), LE can be mathematically expressed as $LE = \frac{RH_a s}{RH_a s + \gamma}\left(R_n - G + \frac{\rho c_p q^*(T_0)}{RH_a s}\frac{RH_0 - RH_a}{r_a}\right)$. The last term of the right-hand side of the PM_{RH} equation, representing the relative humidity flux, plays a significant role in non-equilibrium conditions when the relative humidity difference between the land surface and the atmosphere is significant. In Equation 15, this last term of the PM_{RH} equation is estimated using H_{MEP}, implying that the physical meaning of the H_{MEP} term is correcting the non-equilibrium in the PM_{RH} equation. Indeed, $\frac{RH_0 - RH_a}{r_a}$ is negatively correlated with sensible heat flux in dry conditions (Kim et al., 2021), which justifies the H_{MEP} term in Equation 15.

Similar to the SFE theory, Equation 15 should be applied to time scales longer than daily instead of at a sub-daily time scale since underlying theories are based on the steady state principles, which require some time for converging. Therefore, each variable in Equation 15 should be considered as a time average for daily or longer than daily time scales (e.g., weekly and monthly etc.).

Using Equation 15, ET can be easily estimated by readily obtainable or predictable meteorological information including relative humidity, air temperature, net radiation, soil heat flux, and the radiometric land surface temperature. The land surface temperature is an additional component for ET estimation compared to the SFE theory, and it can be calculated from the outgoing longwave radiation if measurements are available or thermal remote sensing from satellites.

Here, we calculate T_0 as follows:

$$T_0 = (Rl_{out} - Rl_{atm}\,(1 - \varepsilon))/\varepsilon\sigma_{SB})^{1/4} \quad (16)$$

where Rl_{out} is outgoing (upward) longwave radiation observation (W m^{-2}). We used land cover type-specific emissivity (ε) values reported in Feltz et al. (2018) based on the IGBP (The

International Geosphere-Biosphere Programme) land cover classification for each flux site represented in the FLUXNET2015 dataset (Table S1).

After calculating T_0 based on Equation 16, we adjust T_0 for the following conditions since the MEP principle may be not appropriate in these conditions.

$$T_0 - T_a = \begin{cases} T_0 - T_a, & T_a - 1 \le T_0 \le T_a + 10 \\ 0, & T_0 < T_a - 1 \; or \; T_0 > T_a + 10 \end{cases} \quad (17)$$

The MEP principle implicitly assumes positive $T_0 - T_a$ when available radiation energy is positive. Accordingly, we set the lower limit of the land surface temperature as $T_0 \ge T_a - 1$ with a 1 Kelvin buffer to address measurement uncertainty. The upper limit of the land surface temperature (i.e., $T_0 \le T_a + 10$) is introduced since too large $T_0 - T_a$ values do not correspond to the maximum entropy state, as σ declines with increasing r_a (corresponding to increasing $T_0 - T_a$) after the peak (Figure 1) (Kleidon & Schymanski, 2008). For low values of σ, H_{MEP} cannot well constrain sensible heat flux (Figure 2). Therefore, we set this upper limit in Equation 17.

Similarly, we adjust r_{MEP} to reduce possible uncertainties as follows.

$$r_{MEP} = \begin{cases} r_{MEP}, & r_{MEP} \ge \frac{\rho c_p (T_0 - T_a)}{R_n - G} \\ \frac{\rho c_p (T_0 - T_a)}{R_n - G}, & r_{MEP} < \frac{\rho c_p (T_0 - T_a)}{R_n - G} \end{cases} \quad (18)$$

where r_{MEP} on the right-hand side of the equation is aerodynamic resistance for the MEP state in Equation 11, while $\frac{\rho c_p (T_0 - T_a)}{R_n - G}$ is aerodynamic resistance when there is no evaporation. Although conditions meeting $r_{MEP} < \frac{\rho c_p (T_0 - T_a)}{R_n - G}$ are very rare, we introduce this adjustment in order to minimize the possible overestimation of H_{MEP} when true aerodynamic resistance is greater than r_{MEP} in Equation 11.

The final values of $T_0 - T_a$ and r_{MEP} derived from Equations 17 and 18 are used to determine H_{MEP} using Equation 14. Based on this, we estimate *LE* using Equation 15, and this is the proposed ET model, referred to as the SFE-MEP model. In the following sections, we test the proposed model using FLUXNET2015 as the observational dataset.

3 Materials and Methods

The FLUXNET2015 dataset (Pastorello et al., 2020), which includes 212 eddy-covariance flux tower sites around the globe, was used for evaluating the proposed ET model. Latent and sensible heat fluxes, net radiation, soil heat flux, air temperature, relative humidity (or vapour pressure deficit), barometric pressure, incoming longwave radiation, and outgoing longwave radiation were obtained at daily, weekly and monthly scales from the FLUXNET2015 dataset. Eddy-covariance observations of latent heat flux and energy balance corrected latent heat flux based on the Bowen ratio preservation method (Pastorello et al., 2020; Twine et al., 2000) were used as references to evaluate the proposed ET estimation model and the SFE ET estimation.

We only selected periods for which all required variables for ET calculations based on Equation 15 were available. Also, we only included data for periods for which the quality control

flag indicated more than 80% of the half-hourly data were used for generating the daily, weekly, or monthly datasets (i.e., measured data or high quality gap-filled data). We filtered out data points when available energy (i.e., net radiation minus soil heat flux) was negative or latent and sensible heat fluxes were negative. Also, data in which surface energy imbalance (available energy minus the sum of sensible and latent heat flux without energy balance correction) was greater than 50 W m^{-2} were excluded to reduce systematic uncertainty in the observations (Rigden & Salvucci, 2015). Following these filtering processes, 103 flux sites around the globe were retained (Table S1). We remove six additional sites that are located within 35 km of the coast since the SFE theory should be applied to inland continental regions (McColl et al., 2019). Details on this specific 35 km criterion will be discussed in the next section.

The root-mean-square error (RMSE), mean bias (model – observation), and coefficient of determination (R^2) were calculated to evaluate the SFE ET estimates and the proposed SFE-MEP model estimates against measured values. All statistical analyses were conducted using the R statistical language version 4.0.2 (R CORE TEAM, 2020). Also, the bigleaf R package (Knauer et al., 2018) was used to calculate required variables for ET estimations (e.g., T_0 in Equation 16).

4 Results

Across time scales from daily to monthly, the proposed SFE-MEP model (Equation 15) performed consistently better than the SFE theory (Eequation 1) against observed *LE* as shown in Figure 3. In particular, low values of observed daily scale *LE* were overestimated by the SFE theory (e.g., high density of points around $LE_{SFE} \leq 75$, $LE_{obs} = 0$ W m^{-2} in Figure 3d). This difference was eliminated when estimating *LE* with the proposed SFE-MEP model (Figure 3a). Both models showed improved performance when the aggregation time period was increased from daily to monthly; however, model performance using the SFE-MEP model was consistently better than the SFE estimation regardless of time scale.

However, although the proposed SFE-MEP model consistently outperforms the SFE model estimation in terms of RMSE and R^2 across temporal scales, the absolute improvement is small. This may be because the performance of the SFE is already close to the systematic uncertainty of the eddy-covariance observation as demonstrated by McColl and Rigden (2020). Owing to the well-known energy imbalance problem of the eddy-covariance method (i.e., $H + LE < R_n - G$) (Wilson et al., 2002), observed *LE* by eddy covariance is subject to systematic uncertainty. The systematic measurement uncertainty may be revealed by the difference between the observed *LE* and the energy balance residual *LE* (i.e., $R_n - G - H$) (Mauder et al., 2013; McColl & Rigden, 2020). Although we filtered out data points that corresponded to periods with a large energy imbalance (see Methods), the RMSE and R^2 between the observed *LE* and the energy balance residual in our dataset were 21.8 W m^{-2} and 0.82, respectively, for the daily time scale, representing the approximate upper bound on the performance of any ET estimate. In particular, daily *LE* values in semiarid sites are commonly similar to or less than the closure error implying it is difficult to improve model performance (Garcia et al., 2014). Therefore, the RMSE improvement at the daily time scale from 22 W m^{-2} (with $R^2 = 0.67$) using SFE to 20.3 W m^{-2} (with $R^2 = 0.71$) using the SFE-MEP is significant, with the 10% reduction in RMSE resulting in a model uncertainty that approaches the measurement uncertainty for *LE* using the eddy covariance method.

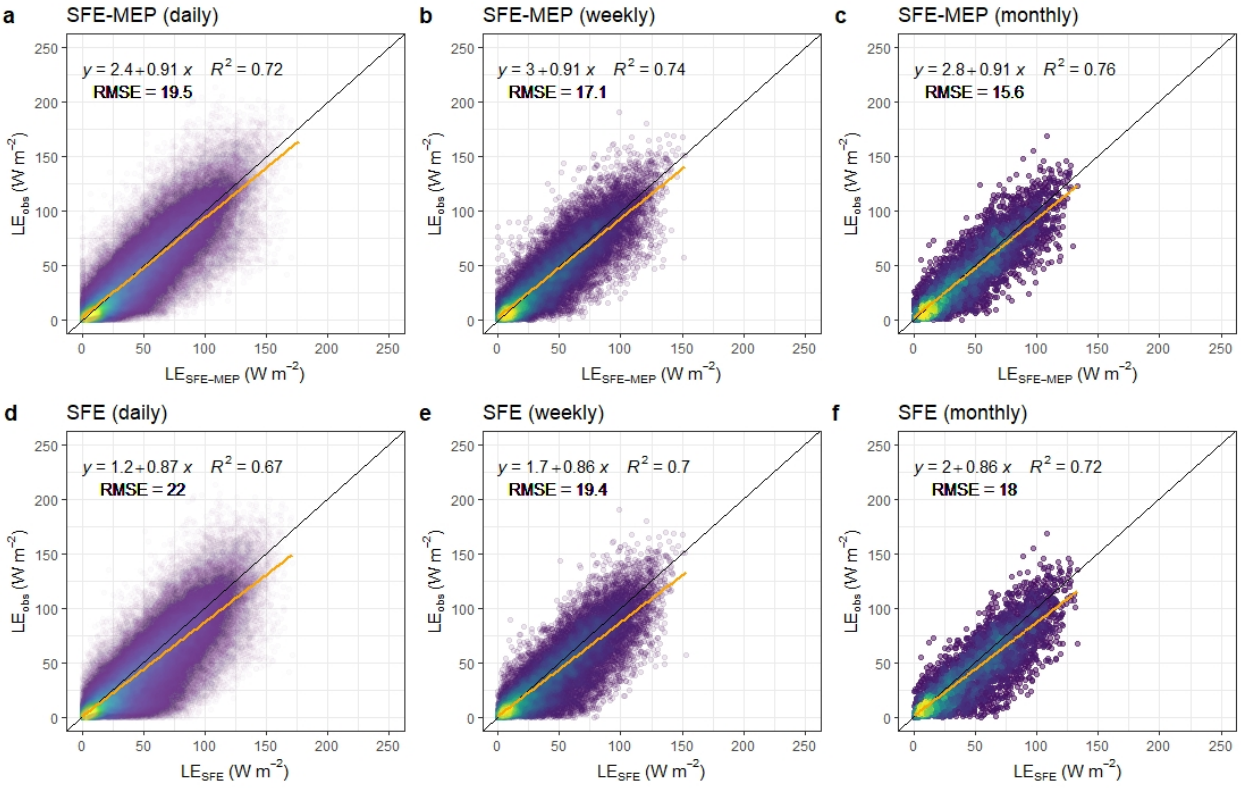

Figure 3. Comparison between eddy covariance *LE* measurements (LE_{obs}) and model-based *LE* estimations using the proposed SFE-MEP model (i.e., Equation 15) ($LE_{SFE\text{-}MEP}$) (a-c), and the SFE model (i.e., equation 1) (LE_{SFE}) (d-f). Each column represents daily (a and d), weekly (b and e), and monthly (c and f) time scales, respectively.

The improved performance of the proposed SFE-MEP model relative to the SFE model is consistent, even if we replace the reference *LE* from the observations with observations for which the energy balance was corrected (i.e., forcing closure of the energy balance based on the Bowen ratio preservation method, which is a technique commonly used in eddy covariance studies (Twine et al., 2000)). Model performance for the SFE-MEP model and SFE relative to observed values with and without forced energy balance closure is summarized in Table 1. In terms of RMSE, bias and R^2, the proposed SFE-MEP model shows better performance than the SFE model across temporal scales against observed *LE*. However, mean bias for the models changes slightly when *LE* observations are adjusted to force energy balance closure in the reference dataset. The SFE-MEP model slightly overestimates uncorrected *LE* observations, while it slightly underestimates *LE* when the energy balance is corrected. Bias for the SFE model also changes based on if the *LE* observations are forced to have energy balance closure or not, with bias values becoming smaller and changing from overestimates without closure to underestimates with energy balance closure.

The slightly underestimated bias for the SFE-MEP model under conditions of forced energy balance closure could be due to a combination of errors in the *LE* model and measurements. Recent evidence suggested that true *LE* may be larger than the uncorrected *LE*

observations and smaller than the energy balance corrected *LE* based on the Bowen ratio preservation method (Mauder et al., 2020). Therefore, the true bias of the SFE-MEP model to true *LE* may be between the biases with the uncorrected *LE* and with the energy balance corrected *LE*. In this case, the absolute value of the mean bias of the proposed model is remarkably small, supporting the accurate performance of the proposed SFE-MEP model.

Table 1. Summary of model performance for *LE* estimation. Two references dataset are used including: eddy covariance *LE* observation and energy balance corrected *LE* (Bowen ratio preservation method). *LE* is estimated by the SFE theory and the proposed SFE-MEP model. Here, units for RMSE and mean bias are in W m^{-2}.

	SFE-MEP model			SFE model		
	RMSE (W m^{-2})	Bias (W m^{-2})	R^2	RMSE (W m^{-2})	Bias (W m^{-2})	R^2
Daily						
LE observation	19.5	1.6	0.72	22	5.6	0.67
Energy balance corrected *LE*	22.3	-4.6	0.74	23.7	-0.6	0.69
Weekly						
LE observation	17.1	1.4	0.74	19.4	5.2	0.70
Energy balance corrected *LE*	18.9	-5.3	0.77	20.1	-1.5	0.72
Monthly						
LE observation	15.6	1.5	0.76	18	5.1	0.72
Energy balance corrected *LE*	17.4	-5.7	0.80	18.7	-2.1	0.74

In order to understand how the proposed SFE-MEP model improves the performance of the SFE estimation by incorporating the H_{MEP} term in Equation 15, we analyzed model bias with respect to volumetric soil water content (VWC) observations (Figure 4). Consistent with a previous study (S. Chen et al., 2021), the SFE model overestimates *LE* when soil moisture is very low (Figure 4b). This poor performance of the SFE model in dry regions can be explained by our theoretical evaluation in the previous section, which shows that it is difficult to approach the equilibrium state in dry regions due to the large time constant required to approach steady state.

This limitation of the SFE theory in dry regions can be reduced by using the proposed SFE-MEP model (Figure 4a) as the proposed model less overestimates *LE* compared to SFE when VWC is very low. Since the SFE-MEP model is constrained by the MEP principle in dry conditions, the overestimation by the SFE theory in dry regions can be reduced. This may be the key reason for the performance improvement obtained using the SFE-MEP model instead of using only SFE theory.

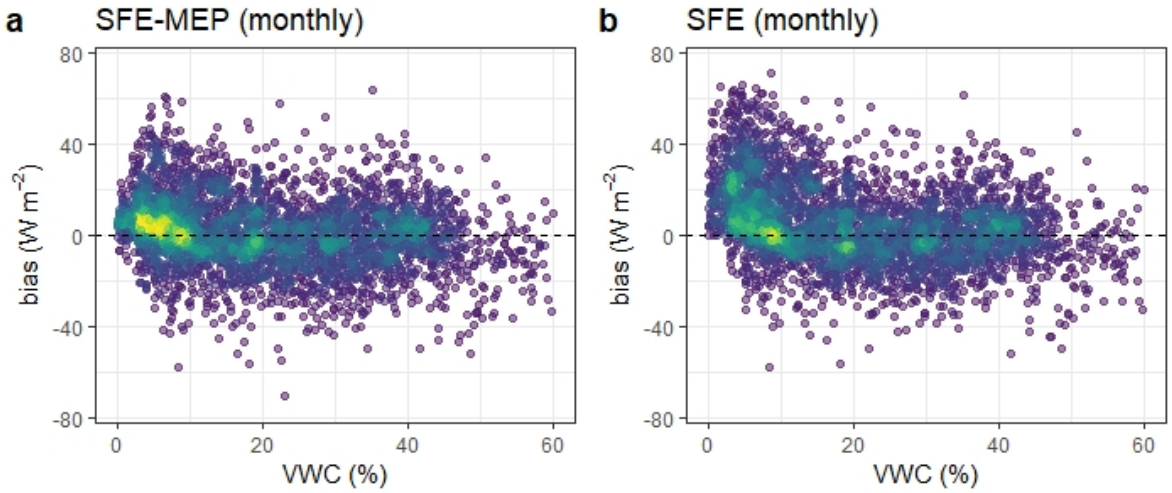

Figure 4. Bias (*LE* estimation - observation) of the SFE-MEP estimation (a) and the SFE estimation (b) as a function of volumetric water content (VWC). Here, monthly scale LE observations (energy balance uncorrected) are used as reference. Sites, which provide VWC observations, are only included in this figure. It should be noted that some wetland sites show saturated VWC, but they are not included here in order to zoom in on the low VWC.

Next, we further analyzed the performance of the SFE theory and the SFE-MEP model by grouping sites according to IGBP land cover types (Figure 5). As we would expect from the VWC analysis, the largest model performance increase was observed for arid and semi-arid regions such as savanna, open shrublands, woody savanna, and closed shrublands. The SFE *LE* estimations showed the poorest performance in these dry regions compared to other land cover types such as forests, which is consistent with our theoretical expectation. This problem is resolved using the SFE-MEP model. The proposed model shows relatively consistent performance with low RMSE values across the land cover types compared to the SFE theory. The performances of the two approaches are similar for the non-dry regions, which is expected since the SFE-MEP model becomes equivalent to the SFE theory.

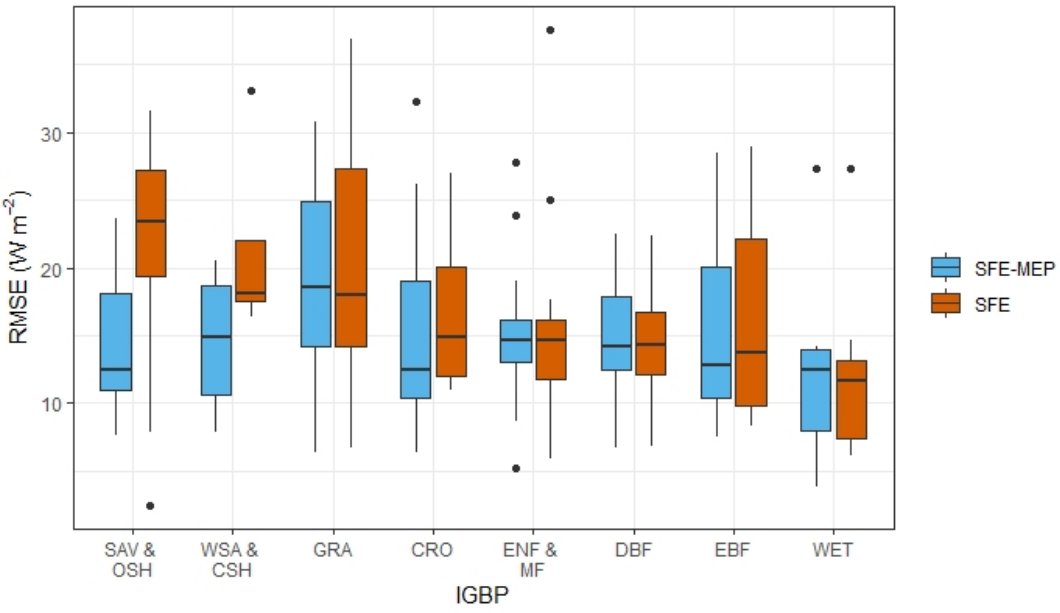

Figure 5. Monthly scale RMSE of the SFE-MEP model and SFE estimations across the land cover types (box plot with outliers). Monthly scale *LE* observations (energy balance uncorrected) are used as reference. The IGBP land cover classification is used for grouping of the sites, which is as follows. SAV & OSH: Savannas and Open Shrublands, WSA & CSH: Woody savanna and Closed Shrublands, GRA: Grasslands, CRO: Croplands, ENF & MF: Evergreen Needleleaf Forests and Mixed Forests, DBF: Deciduous Broadleaf Forests, EBF: Evergreen Broadleaf Forests, WET: Permanent Wetlands.

5 Discussion

We have demonstrated the robustness of SFE theory when applied to ET estimation for most of inland regions, except for conditions for which the land surface is dry and turbulent mixing is weak. To resolve this limitation of the SFE theory in dry regions, we propose to augment SFE theory to include the MEP principle, which is applicable for dry and weak turbulence conditions when SFE theory shows limitations for ET estimation. Based on these theoretical evaluations, we introduce a model that integrates SFE theory and the MEP principle into a single equation, and which is as simple to apply as SFE theory. The two physical theories are complementary to one another in the proposed SFE-MEP model. We have demonstrated that our approach improves the performance of ET estimation compared to using only SFE theory. Using eddy-covariance observations included in the FLUXNET2015 dataset, we have demonstrated the improved performance of the SFE-MEP model compared to SFE, which is particularly improved for dry regions.

Nevertheless, the proposed SFE-MEP model still includes several limitations. Since the proposed model becomes equivalent to the SFE theory except for the arid regions, the proposed SFE-MEP model and SFE theory share similar limitations. In principle, SFE theory only works when the atmospheric state within the ABL is largely determined by latent and sensible heat fluxes at the land surface. If heat fluxes at the top of the ABL significantly affect the ABL state (e.g., strong entrainment), SFE theory can fail to properly estimate ET (McColl & Rigden,

2020). Similarly, SFE theory does not work well for sites close to a coast due to the horizontal advection from the ocean, which decouples the atmospheric state and the land surface heat fluxes (McColl & Rigden, 2020). Indeed, when analyzing the FLUXNET2015 dataset based on distance from a coast, we found low performance for both SFE theory and the SFE-MEP model in matching observed ET for sites located near the ocean (distance from the coast < 35 km; Figure 6).

Unlike SFE theory, the SFE-MEP model is subjected to uncertainty of the radiometric surface temperature (T_0). This may cause a decrease in performance using the SFE-MEP model for some sites compared to SFE theory. Also, field measurement of T_0 is relatively difficult to obtain compared to air temperature although thermal remote sensing from satellites may resolve this problem. In spite of these potential caveats, our theoretical evaluation and the empirical results demonstrated the robustness of the proposed SFE-MEP model across a wide range of environmental conditions. The performance of the SFE-MEP model was consistently better than that obtained using SFE theory, with performance of the SFE-MEP model approaching the measurement uncertainty of the eddy-covariance method, which is particularly notable.

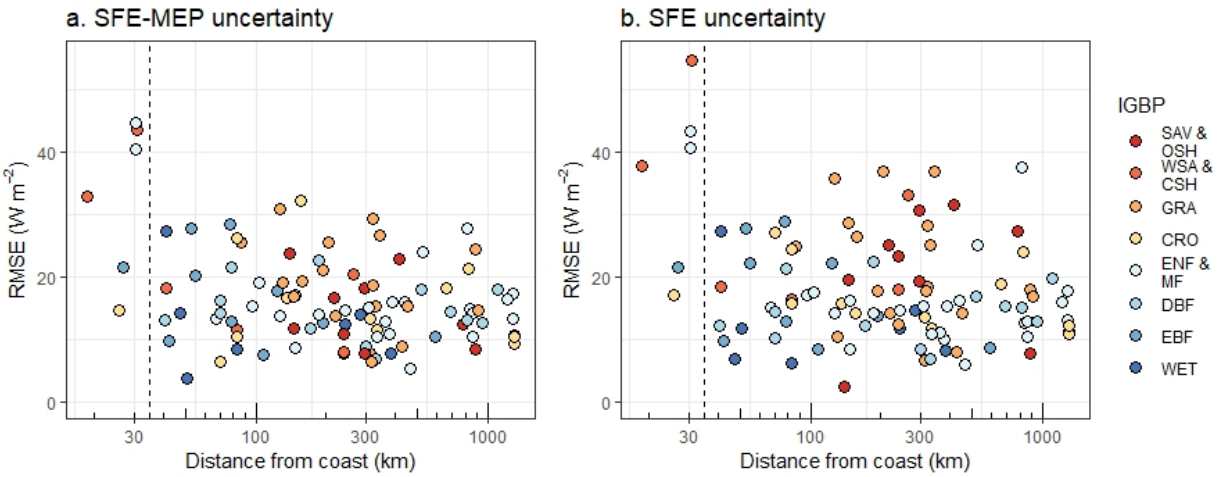

Figure 6. Monthly scale RMSE for each site of the SFE-MEP model (a) and the SFE model (b) as a function of distance from the coast. Filled colours represent the IGBP land cover classification. Monthly scale *LE* observations (energy balance uncorrected) are used as reference. The dashed vertical lines show 35 km from the coast.

6 Conclusions

ET is a key process in the global climate system that links water, energy, and carbon cycles. However, in most Earth-systems models, the relationships linking water, energy, and carbon cycles through ET are parameterized semi-empirically (Short Gianotti et al., 2019). This is particularly problematic in evaluating the Earth system under changing climate conditions, with ET remaining as a major source of uncertainty in the earth-systems models. Unlike common ET estimation approaches which constrain ET using semi-empirically parameterized formulations for aerodynamic resistance and surface resistance, there is no empirical parameters requiring calibration or tuning in our SFE-MEP ET model. Also, the land-atmosphere coupling is

faithfully represented in our model similar to SFE theory. Therefore, the SFE-MEP model can be an alternative or benchmark for evaluating existing or proposed ET models. Also, our SFE-MEP model can be used to analyze trends in ET in that there is no systematic uncertainty that would be introduced through tuning an empirical parameter for a specific time period and then applying the tuned model to other periods. This is particularly important for climate change studies given non-stationarity in future climatic conditions relative to the historical record (Milly et al., 2008). Finally, although we use the radiometric surface temperature observed at the flux tower to evaluate the SFE-MEP model, the SFE-MEP model can be applied to larger spatial scales using radiometric surface temperature obtained from thermal remote sensing derived by satellites such as MODIS, Sentinel 3, Landsat, and ECOSTRESS missions.

559 **Appendix A: Steady state evaporation in an idealized ABL box**

560 Here, we revisit a closed atmospheric boundary layer (ABL) box model (Figure A1). The
561 idealized ABL box does not have diurnal and seasonal variations and it could be interpreted as a
562 time-averaged ABL over a period of time (t). This is conceptually similar to the ABL box model
563 introduced by McColl et al. (2019), but it is simplified further by ignoring relaxation fluxes at the
564 top of the ABL. For the time period t, we presume constant available energy input (i.e., $\frac{d}{dt}(R_n -$
565 $G) = 0$), constant aerodynamic resistance to heat and water vapour transfer (i.e., $\frac{dr_a}{dt} = 0$). The
566 following heat and moisture budget equations govern the closed ABL box system.

567 $$\frac{d\theta_m}{dt} = \frac{H}{\rho c_p h} \quad \text{(A1)}$$

568 $$\frac{dq_m}{dt} = \frac{\gamma LE}{\rho c_p h} \quad \text{(A2)}$$

569 where q_m is the mean specific humidity in the ABL, θ_m is the mean potential temperature
570 in the ABL (K), c_p is the specific heat of air at constant pressure (J kg^{-1} K^{-1}), h is the ABL box
571 height (m), ρ is the air density (kg m^{-3}), γ is psychrometric constant, and t is the time. LE and H
572 are land surface latent and sensible heat fluxes, respectively. In Equations A1 and A2, radiative
573 divergence and horizontal advection are assumed to be negligible following McColl et al. (2019).

574

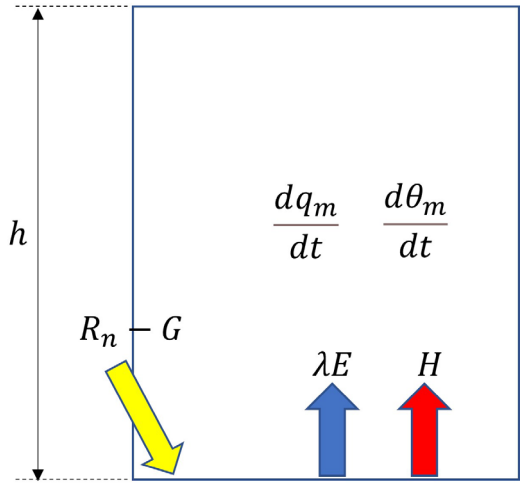

575

576 **Figure A1.** Schematic conceptualization of heat and moisture budgets in the idealized ABL box.
577 R_n represents net radiation based on components of the radiation balance that enter/exit the ABL
578 box.

579

580 Using Equations A1 and A2, we derive Equations 4 and 5. Most previous studies using
581 an ABL box model have applied the "big-leaf" framework for surface resistance to parameterize
582 land surface conditions which resulted in the traditional equilibrium evaporation for a closed
583 system (Culf, 1994; de Bruin, 1983; McNaughton & Jarvis, 1983; McNaughton & Spriggs, 1986;
584 Raupach, 2000, 2001; van Heerwaarden et al., 2009). McColl et al. (2019) also used surface
585 resistance to parameterize land surface. In the present derivation, however, we express
586 evaporation using land surface relative humidity (RH_0) instead of surface resistance and assume

constant RH_0 with time instead of constant surface resistance. This different parameterization is conceptually similar with Li and Wang (2019). Using RH_0, the land surface heat fluxes are expressed as follows.

$$LE = \rho \frac{c_p}{\gamma} \frac{RH_0 q^*(T_0) - q_m}{r_a} \tag{A3}$$

$$H = \rho c_p \frac{T_0 - \theta_m}{r_a} \tag{A4}$$

where q^* is saturation specific humidity, T is temperature, r_a is aerodynamic resistance to water vapour and sensible heat transfer (s m^{-1}). The subscript m indicates the mean atmospheric state in the ABL (including both the surface and mixed layers), and the subscript 0 indicates the land surface. Then, changes of LE and H with respect to time can be expressed as follows.

$$\frac{dLE}{dt} = \frac{RH_0 s}{\gamma} \frac{\rho c_p}{r_a} \frac{dT_0}{dt} - \frac{1}{\gamma} \frac{\rho c_p}{r_a} \frac{dq_m}{dt} \tag{A5}$$

$$\frac{dH}{dt} = \frac{\rho c_p}{r_a} \frac{dT_0}{dt} - \frac{\rho c_p}{r_a} \frac{d\theta_m}{dt} \tag{A6}$$

where $s(= \frac{dq^*}{dT})$ is the linearized slope of saturation specific humidity versus temperature (kg water vapour (kg moist air)$^{-1}$ K^{-1}). In Equations A5 and A6, we assume aerodynamic resistances are constant with time as mentioned above. Since Equations A5 and A6 both include $\frac{\rho c_p}{r_a} \frac{dT_0}{dt}$, we can eliminate $\frac{\rho c_p}{r_a} \frac{dT_0}{dt}$ in equation A5 by substituting equation A6. Therefore, equation A5 can be rewritten as follows

$$\frac{dLE}{dt} - \frac{RH_0 s}{\gamma} \frac{dH}{dt} = \frac{RH_0 s}{\gamma} \frac{\rho c_p}{r_a} \frac{d\theta_m}{dt} - \frac{1}{\gamma} \frac{\rho c_p}{r_a} \frac{dq_m}{dt} \tag{A7}$$

In this ABL box model, we assume $\frac{d}{dt}(R_n - G) = \frac{d}{dt}(H + LE) = 0$. Thus, we can write $\frac{dH}{dt} = -\frac{dLE}{dt}$. Substituting this relationship into the second term of the left-hand side in Equation A7 yields

$$(1 + \frac{RH_0 s}{\gamma}) \frac{dLE}{dt} = \frac{RH_0 s}{\gamma} \frac{\rho c_p}{r_a} \frac{d\theta_m}{dt} - \frac{\rho c_p}{\gamma r_a} \frac{dq_m}{dt}$$

$$\therefore \frac{dLE}{dt} = \frac{\rho c_p}{r_a} \frac{1}{RH_0 s + \gamma} (RH_0 s \frac{d\theta_m}{dt} - \frac{dq_m}{dt}) \tag{A8}$$

Substituting Equations A1 and A2 into equation A8 gives

$$\frac{dLE}{dt} = \frac{\rho c_p}{r_a} \frac{1}{RH_0 s + \gamma} (RH_0 s \frac{H}{\rho c_p h} - \frac{\gamma LE}{\rho c_p h})$$

$$\therefore \frac{dLE}{dt} = \frac{1}{r_a h} \frac{1}{RH_0 s + \gamma} (RH_0 s H - \gamma LE) \tag{A9}$$

Next, we use the energy balance equation $(R_n - G = LE + H)$ to replace H in Equation A9 and rearrange it to give

$$\frac{dLE}{dt} = \frac{1}{r_a h} \frac{1}{RH_0 s + \gamma} [RH_0 s (R_n - G) - (RH_0 s + \gamma) LE]$$

$$\therefore \frac{dLE}{dt} = \frac{1}{r_a h} [\frac{RH_0 s}{RH_0 s + \gamma} (R_n - G) - LE] \tag{A10}$$

616 In order to express $\frac{dLE}{dt}$ using relative humidity at a reference height ($RH_a = \frac{q_m}{q^*(\theta_m)}$)
617 instead of RH_0, we employ the PM$_{RH}$ evaporation model (Kim et al., 2021). The two forms of the
618 PM$_{RH}$ equations for *LE* provides following relationship

619 $$[\frac{RH_0 s}{RH_0 s+\gamma}(R_n - G) - LE] = \frac{q^*(\theta_m)(RH_a s+\gamma)}{q^*(T_0)(RH_0 s+\gamma)}[\frac{RH_a s}{RH_a s+\gamma}(R_n - G) - LE] \quad \text{(A11)}$$

620 Substituting equation A11 into equation A10 yields

621 $$\frac{dLE}{dt} = \frac{1}{r_a h}\frac{q^*(\theta_m)(RH_a s+\gamma)}{q^*(T_0)(RH_0 s+\gamma)}[\frac{RH_a s}{RH_a s+\gamma}(R_n - G) - LE] \quad \text{(A12)}$$

622 The solution of Equation A12 can be obtained by integrating this equation from the initial
623 condition ($LE|_{t=0}$) to time t by assuming that changes in $\frac{RH_a s}{RH_a s+\gamma}(R_n - G)$ and $\frac{1}{r_a h}\frac{q^*(\theta_m)(RH_a s+\gamma)}{q^*(T_0)(RH_0 s+\gamma)}$
624 are negligible over this time scale (McNaughton & Jarvis, 1983).

625 $$LE = \frac{RH_a s}{RH_a s+\gamma}(R_n - G) + [LE|_{t=0} - \frac{RH_a s}{RH_a s+\gamma}(R_n - G)]exp(\frac{-t}{\tau}) \quad \text{(A13)}$$

626 where τ is time constant of the approach to steady state given as follows

627 $$\tau = \frac{q^*(T_0)(RH_0 s+\gamma)}{q^*(\theta_m)(RH_a s+\gamma)} h r_a \quad \text{(A14)}$$

628

629 **Appendix B: Derivation of g_{MEP}**

630 In order to simplify the calculation of $\frac{\partial \sigma}{\partial g_a}$, we rewite Equation 10 as follows:

631 $$\sigma = \frac{\alpha g_a}{(g_a+\beta)^2} \quad \text{(B1)}$$

632 where $\alpha = \frac{\rho c_p}{{T_a}^2}(\frac{R_{ni}-G}{\rho c_p})^2$ and $\beta = \frac{8\varepsilon\sigma_{SB}{T_a}^3}{\rho c_p}$. The partial derivative of σ with respect to g_a can be
633 obtained using the quotient rule.

634 $$\frac{\partial \sigma}{\partial g_a} = \frac{\alpha(g_a+\beta)^2 - 2\alpha g_a(g_a+\beta)}{(g_a+\beta)^4}$$

635 $$\therefore \frac{\partial \sigma}{\partial g_a} = \frac{-\alpha}{(g_a+\beta)^4}({g_a}^2 - \beta^2) = \frac{-\alpha}{(g_a+\beta)^3}(g_a - \beta) \quad \text{(B2)}$$

636 Using Equation B2, we know that $\frac{\partial \sigma}{\partial g_a} = 0$ is equivalent to $g_a - \beta = 0$ because $\frac{-\alpha}{(g_a+\beta)^3}$
637 on the right hand side of Equation B2 is always negative. Therefore, $\frac{\partial \sigma}{\partial g_a} = 0$ is achieved when:

638 $$g_a = \beta = \frac{8\varepsilon\sigma_{SB}{T_a}^3}{\rho c_p} \quad \text{(B3)}$$

639 This solution is the same as Equation 11.

Acknowledgments

We express our thanks to the FLUXNET2015 data providers, site investigators and technicians without who this effort would not have been possible. We acknowledge the support of the Canadian Space Agency (CSA) Grant 21SUESIELH.

Conflict of Interest

The authors declare that they have no conflicts of interest.

Open Research

Data Availability Statement

All data described in the main text are available. The FLUXNET2015 dataset is available from FLUXNET (https://fluxnet.org/data/fluxnet2015-dataset/).

References

Chen, J. M., & Liu, J. (2020). Evolution of evapotranspiration models using thermal and shortwave remote sensing data. *Remote Sensing of Environment, 237*, 111594. https://doi.org/10.1016/j.rse.2019.111594

Chen, S., McColl, K. A., Berg, A., & Huang, Y. (2021). Surface Flux Equilibrium Estimates of Evapotranspiration at Large Spatial Scales. *Journal of Hydrometeorology, 22*(4), 765-779. https://doi.org/10.1175/jhm-d-20-0204.1

Conte, L., Renner, M., Brando, P., Oliveira dos Santos, C., Silvério, D., Kolle, O., et al. (2019). Effects of tropical deforestation on surface energy balance partitioning in Southeastern Amazonia estimated From maximum convective power. *Geophysical Research Letters, 46*(8), 4396-4403. https://doi.org/10.1029/2018gl081625

Culf, A. D. (1994). Equilibrium evaporation beneath a growing convective boundary layer. *Boundary-Layer Meteorology, 70*(1), 37-49. https://doi.org/10.1007/BF00712522

Cuxart, J., & Boone, A. A. (2020). Evapotranspiration over Land from a Boundary-Layer Meteorology Perspective. *Boundary-Layer Meteorology, 177*(2-3), 427-459. https://doi.org/10.1007/s10546-020-00550-9

de Bruin, H. A. R. (1983). A Model for the Priestley-Taylor Parameter α. *Journal of Climate and Applied Meteorology, 22*(4), 572-578. https://doi.org/10.1175/1520-0450(1983)022<0572:amftpt>2.0.co;2

Dewar, R. C. (2005). Maximum entropy production and the fluctuation theorem. *Journal of Physics A: Mathematical and General, 38*(21), L371-L381. https://doi.org/10.1088/0305-4470/38/21/l01

Feltz, M., Borbas, E., Knuteson, R., Hulley, G., & Hook, S. (2018). The Combined ASTER and MODIS Emissivity over Land (CAMEL) Global Broadband Infrared Emissivity Product. *Remote Sensing, 10*(7), 1027. https://www.mdpi.com/2072-4292/10/7/1027

Fisher, J. B., Melton, F., Middleton, E., Hain, C., Anderson, M., Allen, R., et al. (2017). The future of evapotranspiration: Global requirements for ecosystem functioning, carbon and climate feedbacks, agricultural management, and water resources. *Water Resources Research, 53*(4), 2618-2626. https://doi.org/10.1002/2016WR020175

Garcia, M., Fernández, N., Villagarcía, L., Domingo, F., Puigdefábregas, J., & Sandholt, I. (2014). Accuracy of the Temperature–Vegetation Dryness Index using MODIS under water-limited vs. energy-limited evapotranspiration conditions. *Remote Sensing of Environment, 149*, 100-117. https://doi.org/10.1016/j.rse.2014.04.002

Jung, M., Koirala, S., Weber, U., Ichii, K., Gans, F., Camps-Valls, G., et al. (2019). The FLUXCOM ensemble of global land-atmosphere energy fluxes. *Scientific Data, 6*(1), 74. https://doi.org/10.1038/s41597-019-0076-8

Katul, G. G., Oren, R., Manzoni, S., Higgins, C., & Parlange, M. B. (2012). Evapotranspiration: A process driving mass transport and energy exchange in the soil-plant-atmosphere-climate system. *Reviews of Geophysics, 50*(3). https://doi.org/10.1029/2011rg000366

Kim, Y., Garcia, M., Morillas, L., Weber, U., Black, T. A., & Johnson, M. S. (2021). Relative humidity gradients as a key constraint on terrestrial water and energy fluxes. *Hydrol. Earth Syst. Sci., 25*(9), 5175-5191. https://doi.org/10.5194/hess-25-5175-2021

Kleidon, A., & Renner, M. (2018). Diurnal land surface energy balance partitioning estimated from the thermodynamic limit of a cold heat engine. *Earth Syst. Dynam., 9*(3), 1127-1140. https://doi.org/10.5194/esd-9-1127-2018

Kleidon, A., & Schymanski, S. (2008). Thermodynamics and optimality of the water budget on land: A review. *Geophysical Research Letters, 35*(20). https://doi.org/10.1029/2008gl035393

Knauer, J., El-Madany, T. S., Zaehle, S., & Migliavacca, M. (2018). Bigleaf—An R package for the calculation of physical and physiological ecosystem properties from eddy covariance data. *PLOS ONE, 13*(8), e0201114. https://doi.org/10.1371/journal.pone.0201114

Koppa, A., Rains, D., Hulsman, P., Poyatos, R., & Miralles, D. G. (2022). A deep learning-based hybrid model of global terrestrial evaporation. *Nature Communications, 13*(1), 1912. https://doi.org/10.1038/s41467-022-29543-7

Lawrence, D. M., Fisher, R. A., Koven, C. D., Oleson, K. W., Swenson, S. C., Bonan, G., et al. (2020). The Community Land Model Version 5: Description of New Features, Benchmarking, and Impact of Forcing Uncertainty. *Journal of Advances in Modeling Earth Systems, n/a*(n/a). https://doi.org/10.1029/2018ms001583

Lee, X. (2018). *Fundamentals of boundary-layer meteorology* (Vol. 256): Springer.

Li, D., & Wang, L. (2019). Sensitivity of surface temperature to land use and land cover change-Induced biophysical changes: the scale Issue. *Geophysical Research Letters, 46*(16), 9678-9689. https://doi.org/10.1029/2019gl084861

Mallick, K., Toivonen, E., Trebs, I., Boegh, E., Cleverly, J., Eamus, D., et al. (2018). Bridging Thermal Infrared Sensing and Physically-Based Evapotranspiration Modeling: From Theoretical Implementation to Validation Across an Aridity Gradient in Australian Ecosystems. *Water Resources Research, 54*(5), 3409-3435. https://doi.org/doi:10.1029/2017WR021357

Mauder, M., Cuntz, M., Drüe, C., Graf, A., Rebmann, C., Schmid, H. P., et al. (2013). A strategy for quality and uncertainty assessment of long-term eddy-covariance measurements. *Agricultural and forest meteorology, 169*, 122-135. https://doi.org/10.1016/j.agrformet.2012.09.006

Mauder, M., Foken, T., & Cuxart, J. (2020). Surface-Energy-Balance Closure over Land: A Review. *Boundary-Layer Meteorology, 177*(2-3), 395-426. https://doi.org/10.1007/s10546-020-00529-6

McColl, K. A., & Rigden, A. J. (2020). Emergent Simplicity of Continental Evapotranspiration. *Geophysical Research Letters, 47*(6), e2020GL087101. https://doi.org/10.1029/2020gl087101

McColl, K. A., Salvucci, G. D., & Gentine, P. (2019). Surface flux equilibrium theory explains an empirical estimate of water-limited daily evapotranspiration. *Journal of Advances in Modeling Earth Systems, 11*(7), 2036-2049. https://doi.org/10.1029/2019ms001685

McNaughton, K. G., & Jarvis, P. G. (1983). Predicting effects of vegetation changes on transpiration and evaporation. *Water deficits and plant growth, 7*, 1-47.

McNaughton, K. G., & Spriggs, T. W. (1986). A mixed-layer model for regional evaporation. *Boundary-Layer Meteorology, 34*(3), 243-262. journal article. https://doi.org/10.1007/bf00122381

Milly, P. C. D., Betancourt, J., Falkenmark, M., Hirsch, R. M., Kundzewicz, Z. W., Lettenmaier, D. P., & Stouffer, R. J. (2008). Stationarity Is Dead: Whither Water Management? *science, 319*(5863), 573-574. https://doi.org/10.1126/science.1151915

Monteith, J. L. (1981). Evaporation and surface temperature. *Quarterly Journal of the Royal Meteorological Society, 107*(451), 1-27. https://doi.org/10.1002/qj.49710745102

Monteith, J. L., & Unsworth, M. (2013). *Principles of environmental physics: plants, animals, and the atmosphere*: Academic Press.

Pan, S., Pan, N., Tian, H., Friedlingstein, P., Sitch, S., Shi, H., et al. (2020). Evaluation of global terrestrial evapotranspiration using state-of-the-art approaches in remote sensing, machine learning and land surface modeling. *Hydrol. Earth Syst. Sci., 24*(3), 1485-1509. https://doi.org/10.5194/hess-24-1485-2020

Pastorello, G., Trotta, C., Canfora, E., Chu, H., Christianson, D., Cheah, Y.-W., et al. (2020). The FLUXNET2015 dataset and the ONEFlux processing pipeline for eddy covariance data. *Scientific Data, 7*(1), 225. https://doi.org/10.1038/s41597-020-0534-3

Polhamus, A., Fisher, J. B., & Tu, K. P. (2013). What controls the error structure in evapotranspiration models? *Agricultural and forest meteorology, 169*, 12-24. https://doi.org/10.1016/j.agrformet.2012.10.002

R CORE TEAM. (2020). R: A language and environment for statistical computing. *R Foundation for Statistical Computing, Viena, Austria, Vienna, Austria*.

Raupach, M. R. (2000). Equilibrium evaporation and the convective boundary Layer. *Boundary-Layer Meteorology, 96*(1), 107-142. journal article. https://doi.org/10.1023/a:1002675729075

Raupach, M. R. (2001). Combination theory and equilibrium evaporation. *Quarterly Journal of the Royal Meteorological Society, 127*(574), 1149-1181. https://doi.org/10.1002/qj.49712757402

Reichstein, M., Camps-Valls, G., Stevens, B., Jung, M., Denzler, J., Carvalhais, N., & Prabhat. (2019). Deep learning and process understanding for data-driven Earth system science. *Nature, 566*(7743), 195-204. https://doi.org/10.1038/s41586-019-0912-1

Rigden, A. J., & Salvucci, G. D. (2015). Evapotranspiration based on equilibrated relative humidity (ETRHEQ): Evaluation over the continental U.S. *Water Resources Research, 51*(4), 2951-2973. https://doi.org/10.1002/2014wr016072

Short Gianotti, D. J., Rigden, A. J., Salvucci, G. D., & Entekhabi, D. (2019). Satellite and Station Observations Demonstrate Water Availability's Effect on Continental-Scale Evaporative and Photosynthetic Land Surface Dynamics. *Water Resources Research, 55*(1), 540-554. https://doi.org/10.1029/2018WR023726

Trebs, I., Mallick, K., Bhattarai, N., Sulis, M., Cleverly, J., Woodgate, W., et al. (2021). The role of aerodynamic resistance in thermal remote sensing-based evapotranspiration models. *Remote Sensing of Environment, 264*, 112602. https://doi.org/j.rse.2021.112602

Twine, T. E., Kustas, W. P., Norman, J. M., Cook, D. R., Houser, P. R., Meyers, T. P., et al. (2000). Correcting eddy-covariance flux underestimates over a grassland. *Agricultural and forest meteorology, 103*(3), 279-300. https://doi.org/10.1016/S0168-1923(00)00123-4

van Heerwaarden, C. C., Vilà-Guerau de Arellano, J., Moene, A. F., & Holtslag, A. A. M. (2009). Interactions between dry-air entrainment, surface evaporation and convective boundary-layer development. *Quarterly Journal of the Royal Meteorological Society, 135*(642), 1277-1291. https://doi.org/10.1002/qj.431

Wang, J., & Bras, R. L. (2010). An Extremum Solution of the Monin–Obukhov Similarity Equations. *Journal of the Atmospheric Sciences, 67*(2), 485-499. https://doi.org/10.1175/2009JAS3117.1

Wang, J., & Bras, R. L. (2011). A model of evapotranspiration based on the theory of maximum entropy production. *Water Resources Research, 47*(3). https://doi.org/10.1029/2010WR009392

Wang, K., & Dickinson, R. E. (2012). A review of global terrestrial evapotranspiration: Observation, modeling, climatology, and climatic variability. *Reviews of Geophysics, 50*(2). https://doi.org/10.1029/2011RG000373

Wilson, K., Goldstein, A., Falge, E., Aubinet, M., Baldocchi, D., Berbigier, P., et al. (2002). Energy balance closure at FLUXNET sites. *Agricultural and forest meteorology, 113*(1), 223-243. https://doi.org/10.1016/S0168-1923(02)00109-0